The Richtmyer–Meshkov instability in magnetohydrodynamics

V. Wheatley,[1] R. Samtaney,[2] and D. I. Pullin[3]
[1]*School of Mechanical Engineering, University of Adelaide, Adelaide, South Australia 5005, Australia*
[2]*Princeton Plasma Physics Laboratory, Princeton University, Princeton, New Jersey 08543, USA*
[3]*Graduate Aeronautical Laboratories, California Institute of Technology, Pasadena, California 91125, USA*

(Received 8 February 2009; accepted 23 June 2009; published online 25 August 2009)

In ideal magnetohydrodynamics (MHD), the Richtmyer–Meshkov instability can be suppressed by the presence of a magnetic field. The interface still undergoes some growth, but this is bounded for a finite magnetic field. A model for this flow has been developed by considering the stability of an impulsively accelerated, sinusoidally perturbed density interface in the presence of a magnetic field that is parallel to the acceleration. This was accomplished by analytically solving the linearized initial value problem in the framework of ideal incompressible MHD. To assess the performance of the model, its predictions are compared to results obtained from numerical simulation of impulse driven linearized, shock driven linearized, and nonlinear compressible MHD for a variety of cases. It is shown that the analytical linear model collapses the data from the simulations well. The predicted interface behavior well approximates that seen in compressible linearized simulations when the shock strength, magnetic field strength, and perturbation amplitude are small. For such cases, the agreement with interface behavior that occurs in nonlinear simulations is also reasonable. The effects of increasing shock strength, magnetic field strength, and perturbation amplitude on both the flow and the performance of the model are investigated. This results in a detailed exposition of the features and behavior of the MHD Richtmyer–Meshkov flow. For strong shocks, large initial perturbation amplitudes, and strong magnetic fields, the linear model may give a rough estimate of the interface behavior, but it is not quantitatively accurate. In all cases examined the accuracy of the model is quantified and the flow physics underlying any discrepancies is examined. © *2009 American Institute of Physics*. [DOI: 10.1063/1.3194303]

I. INTRODUCTION

The Richtmyer–Meshkov instability (RMI) is important in a wide variety of applications[1] including inertial confinement fusion[2] and astrophysical phenomena.[3] In these applications, the fluids involved may be ionized and hence be affected by magnetic fields. Samtaney[4] demonstrated, via numerical simulations, that the growth of the RMI is suppressed in the presence of a magnetic field. The particular flow studied was that of a shock interacting with an oblique planar contact discontinuity (CD) separating conducting fluids of different densities within the framework of planar ideal magnetohydrodynamics (MHD). It was shown that the suppression of the instability is caused by changes in the shock refraction process at the CD with the application of a magnetic field.[5] These changes prevent the deposition of circulation on the CD.

A more widely studied flow results from a shock wave accelerating a density interface with a single-mode sinusoidal perturbation in amplitude. Our goal is to understand the effect of a magnetic field on this flow when conducting fluids are involved. The magnetic field is again aligned with the motion of the shock. The initial condition for this flow is illustrated in Fig. 1(a). It is characterized by the incident shock sonic Mach number M, the density ratio across the CD, ρ_2/ρ_1, the ratio of the CDs initial amplitude to its wavelength, η_0/λ, the ratio of specific heats, γ, and the nondimensional strength of the applied magnetic field, $\beta^{-1}=B^2/(2p_0)$. Here B is the magnitude of the applied magnetic field and p_0 is the initial pressure in the unshocked regions of the flow. To demonstrate the suppression of the instability in this geometry, the flow was simulated both in the presence and absence of a magnetic field. For both simulations, $M=2$, $\rho_2/\rho_1=3$, $\eta_0/\lambda=0.1$, and $\gamma=5/3$. In the simulation in which a magnetic field is present, $\beta^{-1}=1$. The numerical method used is described in Sec. III D. Time sequences of density and vorticity fields from the simulations without, (i), and with, (ii), an initial magnetic field are shown in Fig. 2. In (i), the transmitted and reflected shocks are clearly visible in the density fields. Note the presence of the transverse waves that are generated downstream of the leading transmitted and reflected shocks in each simulation. It can be seen from Fig. 2(i) that the vorticity generated by the shock refraction process remains at the interface. This causes the interface to roll up into the mushroom shape characteristic of the hydrodynamic RMI. In (ii), the transmitted and reflected fast shocks that are produced by the interaction are clearly visible in the density fields. The tangential velocity jumps across these shocks are considerably smaller than those across the slow shocks; thus they are not as visible in the vorticity fields. The transmitted and reflected slow shocks have small density jumps across them and therefore do not feature prominently in the density fields. It can be seen from the vorticity fields, however, that the majority of the vorticity generated during the shock refraction process is transported away from the interface via the tangential velocity jumps across the slow shocks. In the ideal case, this leaves the

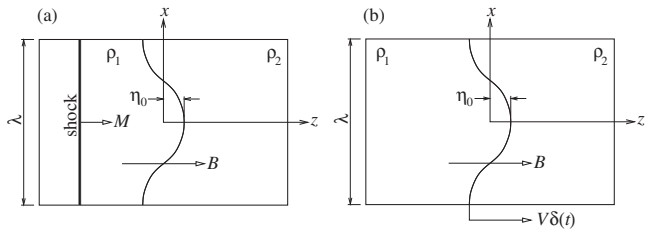

FIG. 1. (a) Initial condition geometry for compressible RMI. (b) Geometry for incompressible model problem.

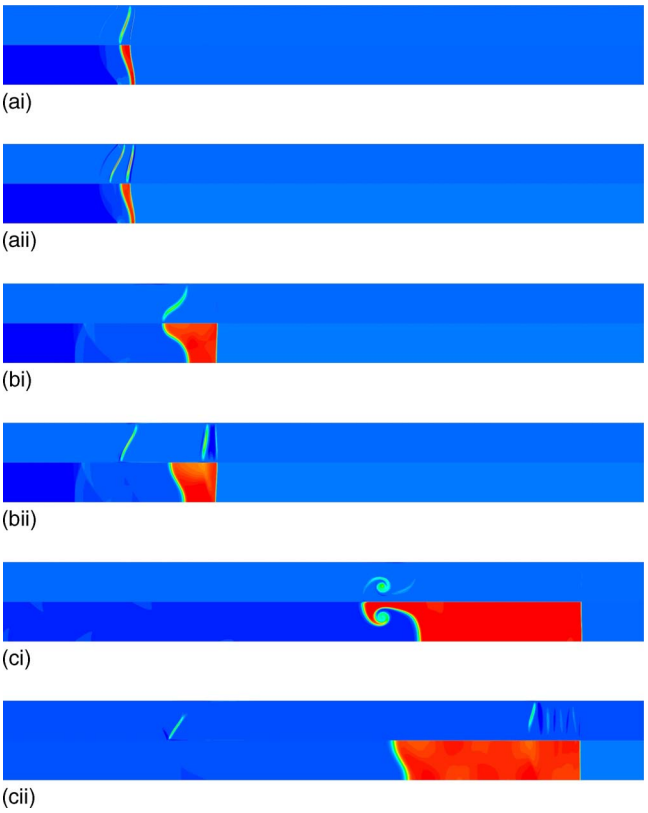

FIG. 2. (Color online) Negative vorticity and density fields from compressible simulations with $M=2$, $\rho_2/\rho_1=3$, $\eta_0/\lambda=0.1$, $\gamma=5/3$, and (i) $B=0$ or (ii) $\beta=1$ at (a) $t/t^*=0.2$, (b) $t/t^*=0.8$, and (c) $t/t^*=3.4$. The top half of each plot shows vorticity while the bottom half shows density. At the time of these images, the incident shock has interacted with the interface.

interface with zero circulation per unit length, which drastically alters its evolution. This is evident from a comparison of Fig. 2(c)(i) and Fig. 2(c)(ii), where the interface from the simulation with a magnetic field present exhibits none of the roll-up seen in the hydrodynamic case.

A second case of interest occurs when the initial magnetic field is parallel to the interface. In this case a jump in tangential velocity across the interface is permitted, allowing the majority of the vorticity generated by the shock refraction process to remain on the interface. Thus the instability may not be suppressed by transport of vorticity. An incompressible model for this case was formulated by Cao *et al.*[6] They determined that when the magnetic field is parallel to the interface and there is no mean shear, the instability is suppressed by a Lorentz force that opposes the perturbation of the interface and no discontinuous waves are generated. As the characteristics of the flow in this case differ substantially from that shown in Fig. 2, we do not consider it any further here.

As a model for this flow in the case where a magnetic field aligned with the shock motion is present, we examined the growth of a sinusoidally perturbed interface separating incompressible conducting fluids that is impulsively accelerated at $t=0$.[7] The setup for the model problem is illustrated in Fig. 1(b). This problem is characterized by ρ_1/ρ^*, ρ_2/ρ^*, η_0/λ, β, and the normalized magnitude of the impulse, $V\sqrt{\rho^*/p_0}$. Appropriate values of V and ρ^* are computed from the corresponding shock driven flow; V is the change in mean interface velocity produced by the shock interaction process, while ρ^* is selected to be the post-interaction value of ρ_1. We shall subsequently refer to this as the incompressible linear theory (ILT). The ILT differs from the full MHD RMI in that it is incompressible, linear, and driven by an impulse rather than by the impact of a shock wave. Here, the performance of the model is assessed for a variety of cases by comparing it to the results of compressible numerical simulations. In each case, an impulse driven linearized (IDL) simulation, a shock driven linearized (SDL) simulation, and a nonlinear (NL) simulation were carried out. This allows the effects on the flow of compressibility, shock acceleration, and nonlinearity to be assessed systematically: differences between the ILT and an IDL simulation are mainly due to the effects of compressibility, differences between IDL and SDL simulations are due to the effects of shock rather than impulsive acceleration, and differences between SDL and NL simulations are due to NL effects.

It is expected that, for fixed γ, the effects of compressibility increase with shock Mach number M, while NL effects increase with the initial amplitude of the interface η_0. From the ILT, the propagation speeds of the fronts that carry circulation away from the interface scale like the Alfvén speed, $C_A=B/\sqrt{\rho}$. This must be small compared to the sound speed, which corresponds to $\beta\equiv 2a^2/\gamma C_A^2$ being large, if these fronts are not to interact with the shocks present in the compressible case. Thus it is anticipated that the ILT will be most accurate for a flow characterized by small M, small η_0, and large β. The performance of the model for such a set of parameters is analyzed as baseline case. We then examine how the performance of the model is affected as M, η_0, and β^{-1} are increased.

In the sequel, we first present the incompressible model for the MHD Richtmyer–Meshkov flow, including features not previously discussed. The numerical methods and simulation setups utilized are described next. Following this, we analyze the results of all methods for a baseline case from which we began our investigations. In this section, we present many finer details of the MHD Richtmyer–Meshkov flow that were not discussed in previous works. The effects of increasing shock strength, magnetic field strength, and perturbation amplitude are then investigated sequentially. After examining the performance of the model for a case where all of these parameters are large, we present the conclusions that have arisen from this investigation.

II. INCOMPRESSIBLE MODEL

The derivation of the incompressible model for the MHD Richtmyer–Meshkov flow was presented in Wheatley *et al.*[7] To derive the model, the linearized equations of ideal, incompressible MHD are solved in a noninertial reference frame that has acceleration $V\delta(t)$ in the z-direction. Here, $\delta(t)$ is the Dirac delta function and $V \ll c$. The equations are linearized about a base flow that results from the impulsive acceleration of an unperturbed interface. Our choice of reference frame results in the horizontal velocity (w) of the base flow being zero for all time. The resulting linearized equations are subject to an impulsive forcing that is nonzero only in a small region between $z=0$ and the perturbed interface location $z=h(x,t)=\eta(t)e^{ikx}(h \ll \lambda)$. All perturbations are assumed to have the form $q'(x,z,t)=\hat{q}(z,t)e^{ikx}$. Subject to boundary and initial conditions, the linearized equations can be solved to yield the following solutions for w in each fluid (see Ref. 7 for details):

$$w_1 = [a_1(t)e^{kz} + H(t+z/C_{A1})c_1(t+z/C_{A1})]e^{ikx}, \tag{1}$$

$$w_2 = [b_2(t)e^{-kz} + H(t-z/C_{A2})d_2(t-z/C_{A2})]e^{ikx}, \tag{2}$$

where $H(z)$ is the Heaviside function. In the above expressions,

$$a_1(t) = K_A\left[\frac{2\alpha_1^2 e^{\alpha_1 t}}{(\alpha_1-\sigma)^2+\tau^2} + \Re\left(\frac{(\sigma+i\tau)(\alpha_1+\sigma+i\tau)e^{(\sigma+i\tau)t}}{i\tau(\sigma+i\tau-\alpha_1)}\right)\right], \tag{3}$$

$$b_2(t) = K_A\left[\frac{2\alpha_2^2 e^{\alpha_2 t}}{(\alpha_2-\sigma)^2+\tau^2} + \Re\left(\frac{(\sigma+i\tau)(\alpha_2+\sigma+i\tau)e^{(\sigma+i\tau)t}}{i\tau(\sigma+i\tau-\alpha_2)}\right)\right], \tag{4}$$

$$c_1(t) = K_C\left[\frac{(\alpha_1+\alpha_2)e^{\alpha_1 t}}{(\alpha_1-\sigma)^2+\tau^2} + \Re\left(\frac{(\alpha_2+\sigma+i\tau)e^{(\sigma+i\tau)t}}{i\tau(\sigma+i\tau-\alpha_1)}\right)\right], \tag{5}$$

$$d_2(t) = K_D\left[\frac{(\alpha_1+\alpha_2)e^{\alpha_2 t}}{(\alpha_2-\sigma)^2+\tau^2} + \Re\left(\frac{(\alpha_1+\sigma+i\tau)e^{(\sigma+i\tau)t}}{i\tau(\sigma+i\tau-\alpha_2)}\right)\right], \tag{6}$$

where

$$\alpha_1 = \frac{Bk}{\sqrt{\rho_1}}, \quad \alpha_2 = \frac{Bk}{\sqrt{\rho_2}}, \quad \sigma = -\frac{Bk(\sqrt{\rho_1}+\sqrt{\rho_2})}{\rho_1+\rho_2}, \tag{7}$$

$$\tau = \frac{[B^2k^2(\rho_1+\rho_2-2\sqrt{\rho_1\rho_2})]^{1/2}}{\rho_1+\rho_2}, \tag{8}$$

and

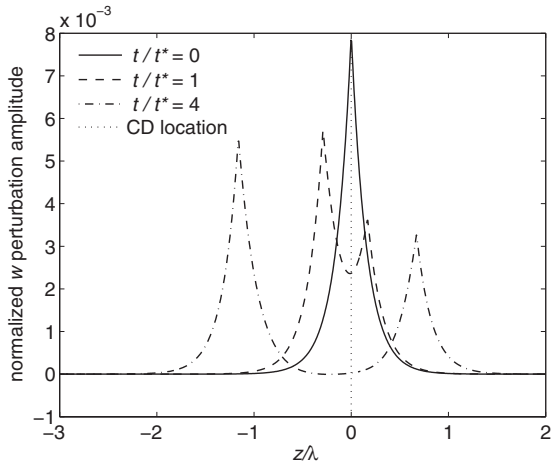

FIG. 3. Profiles of $\hat{w}(z,t)\sqrt{\rho^*/p_0}$ at $t/t^*=0$, $t/t^*=1$, and $t/t^*=4$ for $\rho_1/\rho^*=1.483\ 72$, $\rho_2/\rho^*=4.431\ 59$, $V\sqrt{\rho^*/p_0}=0.319\ 125$, $\eta_0/\lambda=0.007\ 992\ 76$, and $\beta=16$. Here $t^* \equiv \lambda\sqrt{\rho^*/p_0}$. The maxima of $\hat{w}(z,t)$ coincide with the Alfvén fronts.

$$K_A = kV\eta_0\mathcal{A}, \quad K_C = -\frac{2Bk^2V\eta_0\mathcal{A}\rho_2}{\sqrt{\rho_1}\rho_2+\sqrt{\rho_2}\rho_1}, \quad K_D = \frac{\rho_1}{\rho_2}K_C.$$

The Atwood number $\mathcal{A} \equiv (\rho_2-\rho_1)/(\rho_2+\rho_1)$. The above expressions are not valid if $\tau=0$, but this requires that either $B=0$, $k=0$, or $\rho_1=\rho_2$, which corresponds to cases that are not of interest here.

A. Initial solution and growth rate

Profiles of $\hat{w}(z,t)$ at various times are shown in Fig. 3 for one set of parameters. The initial ($t=0^+$) velocity distribution,

$$w(x,z,0^+) = \eta_0 kV\mathcal{A}e^{-k|z|+ikx}, \tag{9}$$

is identical to the steady velocity distribution that arises from the hydrodynamic ($B=0$) case. This implies that the initial growth rate of the interface, which to leading order is given by $\hat{w}_i(0,0)$, is unaffected by the presence of a magnetic field. Indeed, from Eq. (1) or Eq. (2) it can be shown that this initial growth rate is

$$\left.\frac{\partial\eta}{\partial t}\right|_{t=0} = \eta_0 kV\mathcal{A}, \tag{10}$$

as in the hydrodynamic case.[8] This is consistent with the fact that the baroclinic generation of vorticity ω is unaffected by the presence of the magnetic field.

B. Circulation distribution

On any interface with unit tangent $\hat{\mathbf{t}}$, the circulation per unit length Δu is given by

$$\Delta u = [\mathbf{u}\cdot\hat{\mathbf{t}}].$$

For the interfaces in our problem, $\mathbf{u}\cdot\hat{\mathbf{t}}=u$ to leading order. Using the fact that $u=iDw/k$, where D denotes a derivative with respect to z,

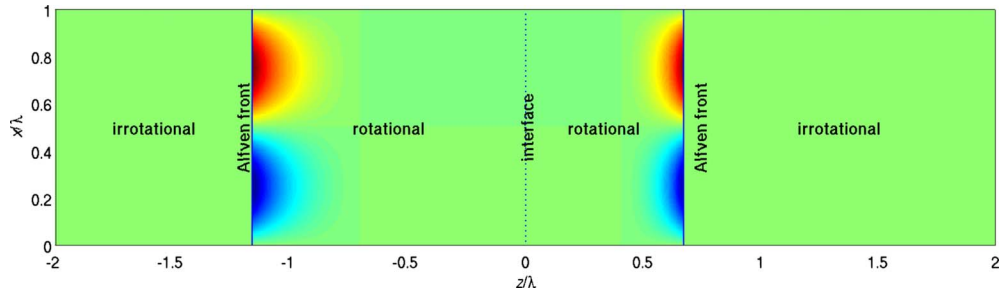

FIG. 4. (Color online) Negative vorticity field at $t/t^*=4$ for $\rho_1/\rho^*=1.483\ 72$, $\rho_2/\rho^*=4.431\ 59$, $V\sqrt{\rho^*/p_0}=0.319\ 125$, $\eta_0/\lambda=0.007\ 992\ 76$, and $\beta=16$. Here $t^*\equiv\lambda\sqrt{\rho^*/p_0}$.

$$\Delta u=[u]=\frac{i}{k}[Dw]=\frac{i}{k}[D\hat{w}]e^{ikx}.$$

Thus the gradient discontinuities in $\hat{w}$ seen in Fig. 3 indicate the presence of interfaces that carry circulation on a half-period. At $t=0^+$, Fig. 3 shows that circulation is present on the density interface at $z=0$. This was baroclinically generated during the impulsive acceleration of the interface. Away from the interface the flow is irrotational at $t=0^+$; thus the total circulation in a half-period of the domain must be equal to

$$\Gamma_{1/2}=\frac{i}{k}[D\hat{w}]_{z=0,\ t=0}\int_0^{\lambda/2}e^{ikx}dx=4\eta_0 V\mathcal{A}. \tag{11}$$

In MHD, the incompressible vorticity equation

$$\frac{\partial\omega}{\partial t}+(\mathbf{u}\cdot\nabla)\omega=(\omega\cdot\nabla)\mathbf{u}+\frac{\nabla\rho\times\nabla p}{\rho^2}+\frac{\nabla\times[(\nabla\times\mathbf{B})\times\mathbf{B}]}{\rho} \tag{12}$$

has an additional term involving the magnetic field. The additional term implies that, even in the absence of baroclinic generation, vortex lines are not necessarily material lines as they are in hydrodynamics. For $t>0^+$, $\hat{w}$ is smooth around $z=0$, indicating that the circulation has been removed from the density interface. Instead, circulation is carried by two fronts that propagate at the local Alfvén speed in each fluid. These fronts correspond to the locations where the Heaviside functions change magnitude.

In the smooth regions of the flow, the vorticity is given by

$$\omega=\frac{\partial u}{\partial z}-\frac{\partial w}{\partial x}=\frac{i}{k}(D^2w-k^2w). \tag{13}$$

By substituting our solution for w into the above equation, we find that the flow is irrotational upstream of the Alfvén fronts in each fluid. Downstream of the Alfvén fronts, however, we find that the vorticity is nonzero. This is illustrated in Fig. 4, which shows the vorticity field for one particular case. Note that the vorticity decays exponentially downstream of each Alfvén front.

C. Interface behavior

The value of $\hat{w}(z,t)$ at $z=0$ is the growth rate of the interface. From Fig. 3, it can be seen that as t increases and the Alfvén fronts propagate away from the interface, carrying away the majority of the vorticity produced by the impulsive acceleration, the growth rate of the interface decays to zero. Thus the instability of the interface is suppressed and its amplitude asymptotes to a constant value. For $t\to\infty$, the interface amplitude tends to

$$\eta_\infty=\eta_0+\int_0^\infty\hat{w}(0,t)dt=\eta_0\left[1+\frac{V}{B}(\sqrt{\rho_2}-\sqrt{\rho_1})\right]. \tag{14}$$

This shows that the change in interface amplitude is inversely proportional to B. Thus for $B\to 0$, $\eta_\infty\to\infty$, which is in agreement with the result from hydrodynamic linear stability analysis.[8] Interestingly, η_∞ is independent of wavenumber. For finite times the interface amplitude is given by

$$\eta(t)=\eta_0+\int_0^t\hat{w}(0,T)dT=\eta_\infty-(\eta_\infty-\eta_0)e^{\sigma t}\cos\ \tau t, \tag{15}$$

where σ and τ are as defined in Eqs. (7) and (8), respectively.

III. SIMULATION TECHNIQUES

A. Numerical method for linearized simulations

The linearized simulations presented here were carried out using a method developed by Samtaney[9] for obtaining numerical solutions to the linearized ideal MHD equations when the base flow is temporally evolving. In this method, the equations of compressible ideal MHD are specialized to two dimensions, x and z. The solution is then assumed to have the form

$$U(x,z,t)=U^o(z,t)+\epsilon\hat{U}(z,t)\exp(ikx),$$

where $\epsilon\ll 1$, $U^o(z,t)$ is an unsteady one-dimensional base flow, and $\epsilon\hat{U}(z,t)\exp(ikx)$ is the perturbation to the base flow. A finite volume upwind approach is adopted to solve for both the base flow and the perturbations. The equations are integrated in time using a third order Total Variation Diminishing Runge–Kutta scheme and the fluxes are evaluated using Roe's method.

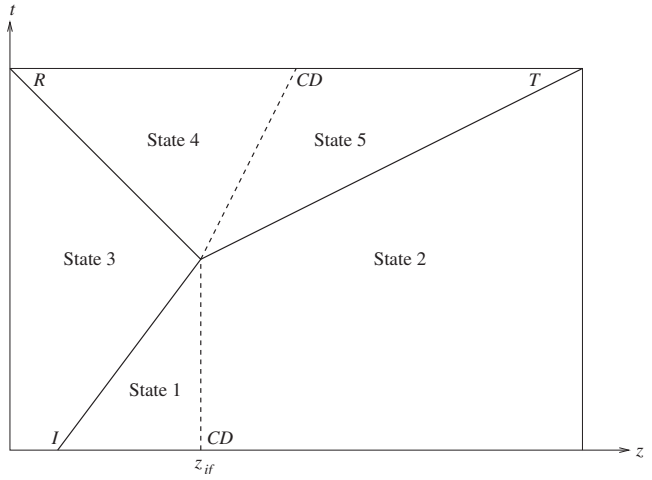

FIG. 5. Illustration of the base flow for SDL simulations in the z-t plane. The lines shown are the paths of the discontinuities in the flow. I, T, and R designate the incident, transmitted, and reflected shocks, respectively, while CD designates the contact discontinuity.

B. Setup for shock driven linearized simulations

Let us first consider the initial conditions for the base flow of a SDL simulation. Prior to the interaction of the incident shock with the density interface, which is unperturbed in the base flow, we designate the quiescent conditions to the left ($z<z_{\mathrm{if}}$) and right ($z>z_{\mathrm{if}}$) of the interface as states 1 and 2, respectively. The conditions downstream of the incident shock are referred to as state 3. For given values of γ and the incident shock Mach number M, state 3 is obtained from the normal shock relations for an ideal gas. For the range of parameters considered herein, the interaction of the incident shock with the interface generates a reflected shock and a transmitted shock. The conditions downstream of the reflected and transmitted shocks are referred to as states 4 and 5, respectively. These states are shown in Fig. 5, which shows the paths of the discontinuities in the base flow in the z-t plane.

In the initial condition for the base flow, the incident shock is represented by a sharp discontinuity located at $z_{\mathrm{shock}}=z_{\mathrm{if}}-\lambda/5$. The flow is initialized to state 3 for $z<z_{\mathrm{shock}}$ and state 1 for $z>z_{\mathrm{shock}}$. For $z>z_{\mathrm{shock}}$, the base flow density is set to

$$\rho^{o}(x,0)=\tfrac{1}{2}\{(\rho_2+\rho_1)+(\rho_2-\rho_1)\tanh[\alpha(z-z_{\mathrm{if}})]\}$$

to represent the density interface. With this initial condition, the base flow for a SDL simulation is the numerical solution to the Riemann problem that arises from the interaction of a shock with an unperturbed density interface. The only nonzero perturbation at $t=0$ is that in density, which approximates a delta function as follows:

$$\hat{\rho}(z,0)=-2\alpha(\rho_R-\rho_L)\frac{\exp[2\alpha(z-z_{\mathrm{if}})]}{\{1+\exp[2\alpha(z-z_{\mathrm{if}})]\}^2}. \tag{16}$$

Here, α is a parameter that regularizes the sharp density interface. It should be chosen judiciously such that the density interface remains relatively sharp with its thickness generally comparable to the numerical smearing of the shock front. As long as this condition is met, the results do not change significantly when α is varied. For our simulations, $\alpha=80$ worked satisfactorily. Note that the initial perturbation amplitude of the interface, η_0, has been scaled out of the problem. For comparison with the results of NL simulations and the ILT, the scaled perturbations from the linearized simulations must be multiplied by η_0.

C. Setup for impulse driven linearized simulations

For IDL simulations, the base flow is initialized to state 4 for $z<z_{\mathrm{if}}$ and state 5 for $z>z_{\mathrm{if}}$. These are the postshock states from the Riemann problem described in Sec. III B. The sharp interface between these two uniform states is approximated by hyperbolic tangent profile, with all quantities having the form

$$q(z,t)=\tfrac{1}{2}\{q_L+q_R+(q_R-q_L)\tanh[\alpha(z-z_{\mathrm{if}})]\},$$

where the subscripts L and R indicate values to the left and right of the interface, respectively. The perturbations are initialized as described in Sec. III B. When scaling the perturbations from IDL simulations for comparison with other results, the initial perturbation amplitude of the interface is taken from the corresponding NL simulation immediately after the interface has been compressed by the passage of the shock wave. These same postshock initial conditions are used in the ILT.

D. Setup for nonlinear simulations

The NL simulations were carried out with a NL compressible MHD solver developed by Samtaney. It uses the eight-wave upwinding formulation of Powell[10] within an unsplit upwinding method.[11] The solenoidal property of the magnetic field is enforced at each time step using a projection method. A constrained transport step is then used to remove divergence modes with a centered finite difference representation. This uses the formulation prescribed by Toth.[12] The setup for the NL simulations is as described in Sec. I, except with different parameter values.

E. Characterization of interface behavior

In the linearized simulations, the interface corresponds to the location where the density perturbation is maximum. The interfacial growth rate $\dot{\eta}$ is approximated by the magnitude of the z-velocity perturbation at this location. The interface amplitude η_{lin} is then computed by numerically integrating $\dot{\eta}$. At time step N, η_{lin} is given by

$$\eta_{\mathrm{lin}}=\eta_0+\sum_{n=1}^{n=N}\dot{\eta}_n\Delta t_n,$$

where the subscript n denotes a quantity is evaluated at the nth time step. For simulations where the interface is shock accelerated, the time origin of the interface amplitude histories is shifted to the point where the amplitude is minimum. This is done to allow direct comparison to the results arising from an impulsive acceleration at $t=0$. The interface amplitude histories obtained from the simulations must be quanti-

tatively compared to the behavior from the ILT, which is given by Eq. (15),

$$\eta(t) = \eta_\infty - (\eta_\infty - \eta_0)e^{\sigma t}\cos\,\pi t.$$

Here, η_∞ is the saturation value of the interface amplitude, while σ governs the saturation timescale. As $|\tau| < |\sigma|$ for $\rho_1 \neq \rho_2$, the oscillations due to the sinusoidal factor are not highly visible. For the simulations, values of these parameters can be estimated by fitting the following function to the amplitude histories:

$$\eta_{\text{fit}}(t) = \eta_\infty - (\eta_\infty - \eta_0)e^{\sigma(t-t_0)}\cos\,\tau(t-t_0). \tag{17}$$

This is done using a NL least-squares fitting routine that determines the values of η_∞, σ, and t_0 that minimize the L_2 norm of the residuals between the data from the simulations and the fitted function. τ is set to the appropriate value from the ILT. If we attempt to determine τ via the fitting routine, values of σ and τ are determined such that the fitted function captures the first of the long period oscillations that occur in interface amplitude history from the NL simulation (η_{NL}). It is shown in Sec. IV, however, that these oscillations are due to the pressure field induced by the interaction of transverse waves downstream of the transmitted and reflected shocks or the reflection of outgoing waves from the shocks. These shocks are not present in the ILT; hence the oscillations should not appear in a fitted function that has the same form as the model η history.

IV. RESULTS

A. Results for a baseline case

As a baseline case, we will study a shock accelerated interface with $M=1.1$, $\beta=16$, $\rho_2/\rho_1=3$, $\eta_0/\lambda=0.01$, and $\gamma=5/3$. In Secs. IV B–IV D, we will investigate the effects of M, β, and η_0/λ on the performance of the ILT by individually varying them from their baseline values and comparing the results to those presented in this section. Note that in all cases presented here, the reflected wave in the base flow is a shock. We have also compared the ILT to simulation results for cases where the reflected wave is a rarefaction. The accuracy of the ILT for these cases was found to be similar to that for the reflected shock cases. The linearized simulations of the baseline case were carried out in the domain $-10\lambda \leq z \leq 10\lambda$, which was discretized into $N_z=3200$ control volumes in the z-direction. The simulations were run for $N_t=6000$ time steps with a Courant–Friedrichs–Lewy (CFL) number of $\lambda_{\max}\Delta t/\Delta x=0.5$, where $\lambda_{\max}$ is the maximum eigenvalue of the system, Δt is the time step, and Δx is the side length of each control volume. All linearized simulations discussed herein were carried out with the same domain, discretization, and CFL number, unless otherwise noted. For the NL simulation of the baseline case, $L_z=12\lambda$, $z_{\text{if}}=7.06\lambda$, $N_x=128$, and $N_z=3072$, where L_i is the length of the domain in the i-direction. The simulation was run with a CFL number of 0.7 for the duration $T_{\text{sim}}/t^*=5.6$, which is approximately double the time the ILT predicts for the interface to reach 99% of its final amplitude, t_{99}. All NL simulations discussed here were run with $L_x=\lambda/2$ and this CFL number for a duration that is approximately $2t_{99}$, unless otherwise noted. A NL simulation was also run with half the resolution in each direction to establish the insensitivity of the η history to the grid. It is important to note that as we are solving a set of equations with no physical dissipation mechanism to set a minimum length scale, we do not expect uniform pointwise convergence toward the weak solution with increasing resolution. Note that the η histories from the NL simulations are filtered to remove spurious, time-step scale oscillations before plotting.

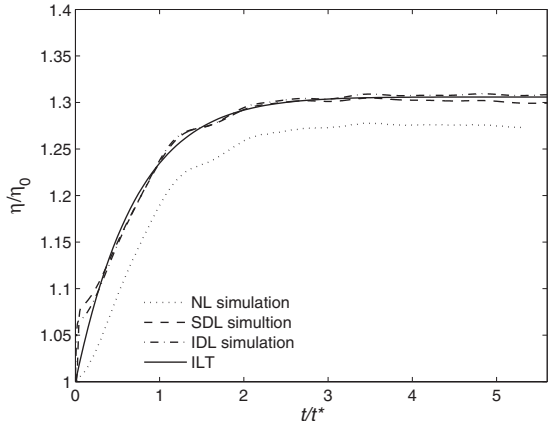

FIG. 6. Interface amplitude histories from the ILT and an IDL simulation, both with $\rho_1/\rho^*=1.192\,23$, $\rho_2/\rho^*=3.575\,29$, $V\sqrt{\rho^*/p_0}=0.135\,324$, $\eta_0/\lambda=0.009\,047\,08$, and $\beta=16$, and both SDL and NL compressible simulations of a shock accelerated interface with $M=1.1$, $\beta=16$, $\rho_2/\rho_1=3$, $\eta_0/\lambda=0.01$, and $\gamma=5/3$.

1. Interface evolution

Figure 6 shows the η histories from the ILT and the three simulations for the baseline case. The model η history is given by Eq. (15). The values of η_∞ and σ computed from these are shown in Table I. The histories from the linearized simulations deviate from both the ILT and the NL simulation for a brief period just after the interface is accelerated. This may be due to the approximate initial density perturbation used in the linearized simulations, which is given by Eq. (16). There is close agreement between the behavior of the interface predicted by the ILT and the IDL simulation, with the final interface amplitudes being within approximately 0.2% of each other. The values of σ, which governs the time to saturation, agree to within 7.2%. The main difference between the two histories is the presence of small amplitude oscillations in the simulation result, the source of which will be discussed in Sec. IV A 2. The amplitude of these oscillations appears to decay with time and they are also seen in the histories from the SDL and NL simulations. Comparing the histories from the IDL and SDL simulations gives an indica-

TABLE I. Interface perturbation parameters from the ILT and simulations corresponding to a shock accelerated interface with $M=1.1$, $\beta=16$, $\rho_2/\rho_1=3$, $\eta_0/\lambda=0.01$, and $\gamma=5/3$.

	Model	IDL simulation	SDL simulation	NL simulation
η_∞/λ	0.011 723 7	0.011 746 5	0.011 641 3	0.011 464 4
σt^*	−1.389 82	−1.289 69	−1.420 71	−1.314 02

tion of the effect of the interface being shock accelerated rather than impulsively accelerated. The qualitative behavior of the interface is similar in both cases, but the shock acceleration appears to result in a slight reduction in the growth of the interface amplitude, with η_∞ being reduced by approximately 0.9%. In addition, the amplitudes from both the shock driven simulations is decreasing slightly near the end of the simulations. This is part of a long period oscillation. In the hydrodynamic case, oscillations in growth rate are known to be caused by the pressure field induced by the interactions of transverse waves downstream of the transmitted and reflected shocks.[1] In addition, the oscillations may also be due to the reflection of outgoing waves from the shocks, which will be discussed in Sec. IV A 2. Comparing the histories from the SDL and NL simulations indicates that the main effect of nonlinearity on the evolution of the interface is a significant decrease in its growth, with η_∞ being approximately 1.5% less in the NL simulation. The cause of the lower interface amplitudes in the NL simulation appears to be the low growth rates that occur immediately after the acceleration of the interface, which are significantly lower than those predicted by the ILT. Low growth rates at early times also occur in the absence of a magnetic field.[13] It was observed that the growth rate is initially mitigated, then increases close to the constant value predicted by the hydrodynamic impulse model of Richtmyer.[8] The results of compressible linear models indicate that this behavior is typical of the RMI[1] and is expected as the impulse model predicts the asymptotic growth rate after the shocks are sufficiently far from the interface.[8] The low growth rates at early times do not significantly affect the extent to which the interface develops in the hydrodynamic case as the growth rate is then approximately constant until the interface enters the NL phase of its development. When a magnetic field is present, however, mitigation of the growth rate at early times significantly reduces the final amplitude of the interface as this is when the growth rate is predicted to be at its maximum.

2. Velocity profiles

Profiles of u' and w' from the ILT and the IDL simulation of the baseline case are shown in Fig. 7 for $t/t^*=4$. The model u' profiles are computed from the w' profiles using the linearized continuity equation and the form of the perturbations as follows:

$$u' = -\frac{1}{ik}\frac{\partial w'}{\partial z}.$$

The profiles of u' and w' are plotted at locations where the perturbation amplitudes are maximum, at $x=\lambda/4$ and $x=0$, respectively. Additional waves can clearly be seen in the profiles from the IDL simulation. The leading edges of these waves propagate outward from the interface at the fast characteristic speed in each fluid. In this case, where the waves are propagating parallel to the base flow magnetic field, the fast characteristic speed corresponds to the sound speed $a_i=\sqrt{\gamma p_0/\rho_i}$, while both the slow and intermediate characteristic speeds are equal to the Alfvén speed $C_{Ai}=B/\sqrt{\rho_i}$. It can

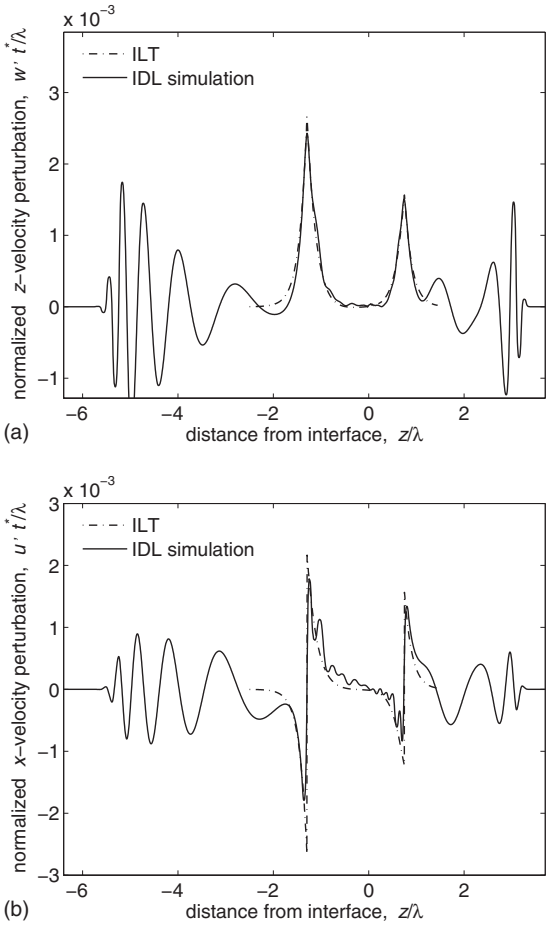

FIG. 7. Profiles of (a) w' at $x=0$ and (b) u' at $x=\lambda/4$ at $t/t^*=4$ from the ILT and the IDL simulation corresponding to a shock accelerated interface with $M=1.1$, $\beta=16$, $\rho_2/\rho_1=3$, $\eta_0/\lambda=0.01$, and $\gamma=5/3$.

be seen from Fig. 8(a) that the additional waves are compressible as the density perturbations associated with them are nonzero; hence they cannot be represented in the incompressible linear model. The amplitudes of the velocity perturbations associated with the compressible waves are comparable to those associated with the model. Despite this, Fig. 6 shows that the ILT is able to predict the evolution of the interface in the IDL simulation quite accurately. The reason for this is that the behavior of the interface is governed by the vorticity distribution and the compressible waves do not have any vorticity associated with them, as can be seen from Fig. 8(b). The vorticity field from the simulation is dominated by the two peaks that approximately coincide with the locations of the Alfvén fronts in the ILT. Figure 7 shows that the flow in this region and around the interface, particularly w', is well represented by the Alfvén fronts and the incompressible flow field from the ILT, although it does not capture the small amplitude waves that appear near the interface.

Since the perturbations have a sinusoidal variation in x, then the value of w' at $z=0$ in the plotted profiles corresponds to the growth rate of the interface. Thus, when a wave with a w perturbation associated with it crosses the interface, it will cause a small oscillation in the interface amplitude. This is the cause of the oscillations that were noted earlier in the η histories from the compressible simu-

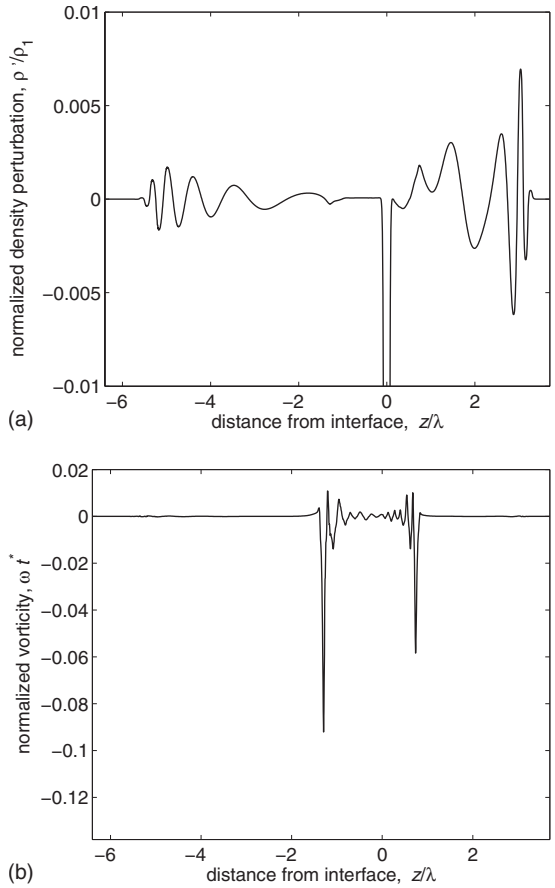

FIG. 8. Profiles of (a) ρ' at $x=0$ and (b) ω at $x=\lambda/4$ at $t/t^*=4$ from the IDL simulation corresponding to a shock accelerated interface with $M=1.1$, $\beta=16$, $\rho_2/\rho_1=3$, $\eta_0/\lambda=0.01$, and $\gamma=5/3$.

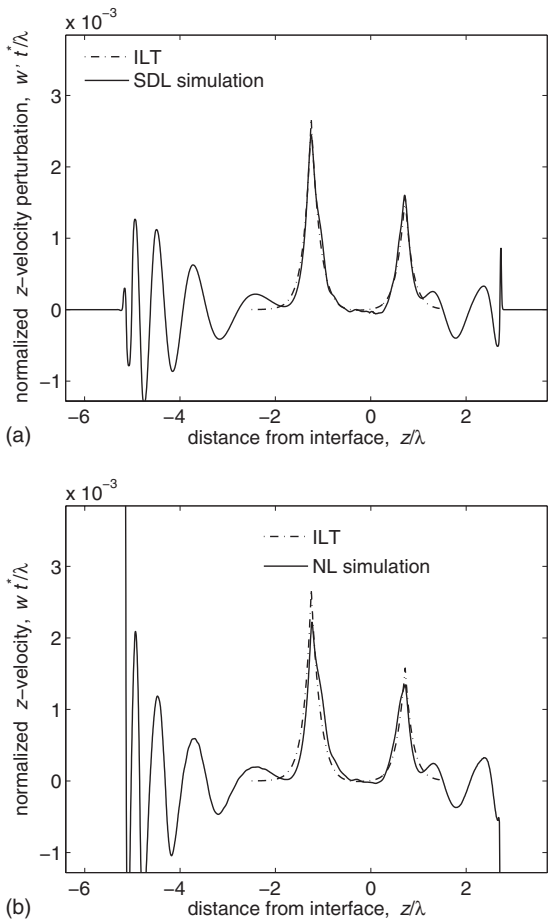

FIG. 9. Velocity profiles at $x=0$ and $t/t^*=4$ from the ILT and shock driven simulations of a shock accelerated interface with $M=1.1$, $\beta=16$, $\rho_2/\rho_1=3$, $\eta_0/\lambda=0.01$, and $\gamma=5/3$. In (a) w' from the SDL simulation is shown while (b) shows w from the NL simulation.

lations. In the IDL simulation, these oscillations decay with time as the high amplitude compressible waves propagate away from the interface at the beginning of the simulation and do not return.

Profiles of w' from the ILT and the SDL simulation of the baseline case are shown in Fig. 9(a) at $t/t^*=4$ in the simulation. The profiles from the ILT are shown at $t/t^*=4-(z_{\text{if}}-z_{\text{shock}})/(M\sqrt{\gamma})$, the approximate time after the acceleration of the interface in the simulation, because the acceleration occurs at $t=0$ in the model. This adjustment is made whenever the ILT is compared to the results of a shock driven simulation. In the SDL simulation, the perturbations are restricted to the region between the two shocks in the base flow. The base flow downstream of the shocks is subsonic with respect to the fast characteristic speed; thus the compressible waves in the solution can catch up to the shocks and interact with them. This process can be seen occurring on the right side of Fig. 9(a). The interaction of the waves with the shock can only produce reflected waves. The flow upstream of the shocks is supersonic with regard to the fast characteristic speed. Figure 9 shows that the ILT reproduces the flow field around the interface from the SDL simulation with approximately the same accuracy as for the IDL simulation.

Profiles of w in the reference frame of the interface from the ILT and the NL simulation of the baseline case are shown in Fig. 9(b) for $t/t^*=4$. Because the full z-velocity is plotted, the transmitted and reflected fast shocks are visible in the profile from the NL simulation. By comparing Fig. 9(b) with Figs. 7 and 9(a), it can be seen that the flow around Alfvén fronts from the ILT does not predict the flow in that region from the NL simulation as accurately as it did for the linearized simulations. This is most likely because in the NL simulation the discontinuities downstream of the fast shocks are not Alfvén fronts but include NL discontinuous waves. These may be slow or intermediate shocks, 180° rotational discontinuities, slow-mode expansion fans, compound waves, or combinations of these.[5] The performance of ILT depends on how well the Alfvén fronts approximate the NL discontinuous waves that are present in the NL simulation. However, the type of waves present varies with position along the interface, as the shock refraction process varies with the incidence angle and with time as they propagate outward and evolve, making it difficult to assess the performance of the ILT in this fashion. For this reason we assess the performance of the ILT based on how well it predicts the overall evolution of the interface, as shown in Fig. 6.

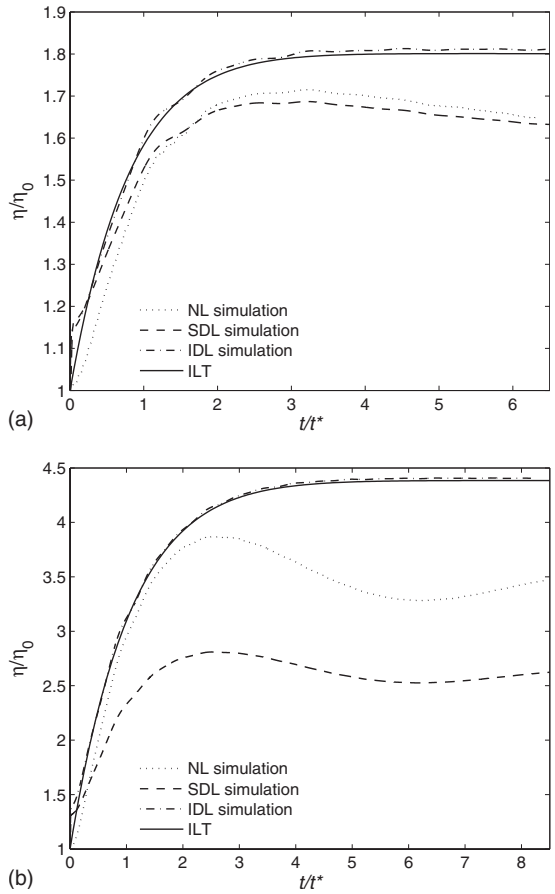

FIG. 10. Interface amplitude histories from the ILT, IDL, SDL, and NL compressible simulations corresponding to a shock accelerated interface with $\beta=16$, $\rho_2/\rho_1=3$, $\eta_0/\lambda=0.01$, $\gamma=5/3$, and (a) $M=1.25$ or (b) $M=2$.

B. Effect of increased shock strength

In this section the effect of increasing the incident shock Mach number M is examined. This is done by studying two additional cases with $M=1.25$ and $M=2$. The other parameters are the same as in the baseline case. Figure 10 shows the η histories from the ILT and the three simulations for the $M=1.25$ and $M=2$ cases (refer to Fig. 6 for the $M=1.1$ case). The values of η_∞ and σ computed from these are shown in Table II along with the simulation parameters.

From Fig. 10, it can be seen that the agreement between the η histories from ILT and the IDL simulation does not degrade as the magnitude of the impulse, V, is increased with M. Thus the linear dependence of $\eta_\infty-\eta_0$ on V predicted by the ILT also appears to hold in the compressible case. The η histories from the IDL and SDL simulations diverge as M increases, indicating that approximating the result of the shock interaction process as an impulsive acceleration becomes less accurate as the shock strength increases. The η histories from the SDL and NL simulations also diverge as M increases, indicating that nonlinearities become more dominant as the shock strength increases. It is apparent from Fig. 10 that in the shock driven η histories, the amplitude of the long period oscillations, relative to $\eta_\infty-\eta_0$, increases with M. As discussed earlier, these oscillations appear to be due to disturbances caused by the interaction of transverse waves downstream of the reflected and transmitted shocks or outgoing waves that have been reflected from the shocks. An example of such a disturbance crossing the interface can be seen in Fig. 11, which shows profiles of w from the $M=2$ NL simulation at three different times. At $t/t^*=6.4$, the disturbance appears as the small peak in w between the two large peaks that bracket the interface, which is located at $z=0$. The disturbance approaches $z=0$ from the right and increases the growth rate of the interface as it crosses it. This event corresponds to the change from negative to positive growth seen in the η history near $t/t^*\approx 6.2$. The increase in amplitude of the oscillations in η with M therefore indicates an increase in the effect of transverse and/or reflected waves, which is consistent with compressibility effects becoming more dominant.

TABLE II. Interface perturbation parameters from the ILT and simulations corresponding to a shock accelerated interface with varying M and $\beta=16$, $\rho_2/\rho_1=3$, $\eta_0/\lambda=0.01$, and $\gamma=5/3$. For the linearized simulations $N_t=4000$. For the NL simulation of the $M=1.25$ case, $L_z=13\lambda$, $z_{if}=6.8\lambda$, $N_x=128$, $N_z=3328$, and $T_{sim}/t^*=6.5$, while for the $M=2$ case, $L_x=\lambda/2$, $L_z=20.5\lambda$, $z_{if}=5.75\lambda$, $N_x=128$, $N_z=5248$, and $T_{sim}/t^*=8.5$.

M	Model	IDL simulation	SDL simulation	NL simulation
		η_∞/λ		
1.1	0.011 723 7	0.011 746 5	0.011 641 3	0.011 464 4
1.25	0.014 425 8	0.014 514 2	0.013 363 5	0.013 561 7
2.0	0.026 500 9	0.025 733 1	0.015 436 1	0.020 605 1
		σt^*		
1.1	−1.389 82	−1.289 69	−1.420 71	−1.314 02
1.25	−1.248	−1.170 46	−1.449 87	−1.465 07
2.0	−0.938 511	−0.907 09	−1.763 15	−1.739 81

Figure 12 shows profiles of w in the reference frame of the interface from the ILT and the NL simulations of the $M=1.25$ and $M=2$ cases. These show that as M is increased, ILT is less able to accurately represent the primary features of the flow, resulting in the increasing disagreement between the interface statistics from the model and the shock driven simulations seen in Table II. For $M=1.25$, ILT overpredicts

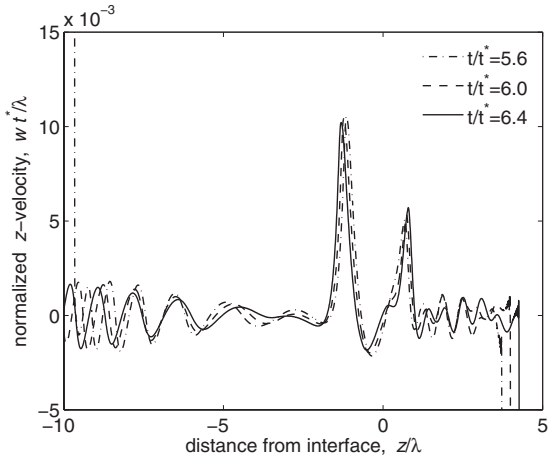

FIG. 11. Profiles of w at $x=0$ in the reference frame of the interface from the NL simulation of a shock accelerated interface with $M=2$, $\beta=16$, $\rho_2/\rho_1=3$, $\eta_0/\lambda=0.01$, and $\gamma=5/3$.

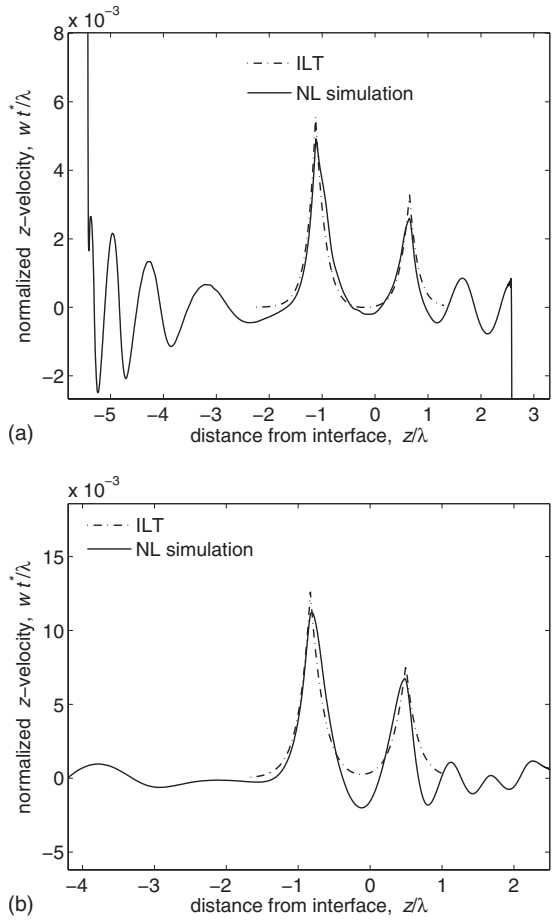

FIG. 12. Profiles of w at $x=0$ in the reference frame of the interface at $t/t^*=4$ from the ILT and NL simulations corresponding to shock accelerated interfaces with $\beta=16$, $\rho_2/\rho_1=3$, $\eta_0/\lambda=0.01$, $\gamma=5/3$, and (a) $M=1.25$ or (b) $M=2$.

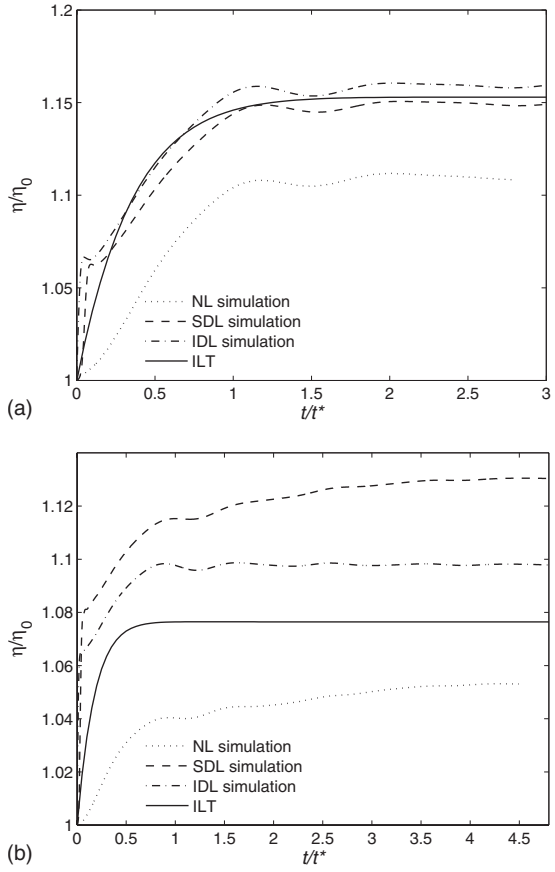

FIG. 13. Interface amplitude histories from ILT, IDL, SDL, and NL compressible simulations corresponding a shock accelerated interface with $M=1.1$, $\rho_2/\rho_1=3$, $\eta_0/\lambda=0.01$, $\gamma=5/3$, and (a) $\beta=4$ or (b) $\beta=1$.

η_∞ from the IDL, SDL, and NL simulations by -0.61%, 0.74%, and 0.60%, respectively, while σ is underestimated by -6.2%, 16.2%, and 17.4%, respectively. For $M=2$, ILT overpredicts η_∞ from the IDL, SDL, and NL simulations by 2.9%, 41.8%, and 22.2%, respectively, while σ is underestimated by -3.3%, 87.9%, and 85.4%, respectively. Taking η_∞ values from the NL simulations to be the desired output of the model, the error in the ILT exceeds 20% for $M>1.71$ for the cases studied here.

C. Effect of increased magnetic field

In this section the effect of increasing the magnetic field magnitude B is examined. This is done by studying two additional cases with $\beta=4$ and $\beta=1$. The other parameters are the same as in the baseline case. Figure 13 shows the η histories from ILT and the three simulations for the $\beta=4$ and $\beta=1$ cases. The values of η_∞ and σ computed from these are shown in Table III.

For $\beta=4$, the agreement between ILT and the linearized simulations remains reasonable, with η_∞ deviating from the predicted value by 0.56% and 0.40% in the IDL and SDL simulations, respectively. The deviations in σ are 14.5% and 17.9%, respectively. The differences between ILT and the NL simulation increase more substantially, with η_∞ and σ deviating by 3.6% and 25.4% from their predicted values, respectively. As $\beta\equiv 2p_0/B^2=2(a/C_A)^2/\gamma$ is decreased further, the Alfvén speed C_A in the undisturbed flow approaches the acoustic sound speed a and they become equal at $\beta=2/\gamma=6/5$. Thus for the $\beta=1$ case, in the undisturbed flow C_A is greater than a and is therefore the fast and intermediate characteristic speed, while a is the slow characteristic speed.

TABLE III. Interface perturbation parameters from ILT and simulations corresponding to a shock accelerated interface with varying β and $M=1.1$, $\rho_2/\rho_1=3$, $\eta_0/\lambda=0.01$, and $\gamma=5/3$. For the NL simulation of the $\beta=4$ case, $L_z=6\lambda$, $z_{\text{if}}=3.53\lambda$, $N_x=256$, $N_z=3072$, and $T_{\text{sim}}/t^*=3$. For the $\beta=1$ case, $L_x=\lambda/2$, $L_z=9.5\lambda$, $z_{\text{if}}=5.59\lambda$, $N_x=128$, $N_z=2432$, and $T_{\text{sim}}/t^*=4.8$. This simulation was run for longer than $2t_{99}\approx 1.4$ because the value of η_∞ was not apparent at that time.

β	Model	IDL simulation	SDL simulation	NL simulation
		η_∞/λ		
16	0.011 723 7	0.011 746 5	0.011 641 3	0.011 464 4
4	0.010 397 5	0.010 456 1	0.010 355 9	0.010 021 9
1	0.009 750 63	0.009 943 64	0.010 202 1	0.009 491 06
		σt^*		
16	−1.389 82	−1.289 69	−1.420 71	−1.314 02
4	−2.779 63	−2.375 5	−2.281 34	−2.073 66
1	−5.559 27	−2.894 82	−2.849 95	−2.401 85

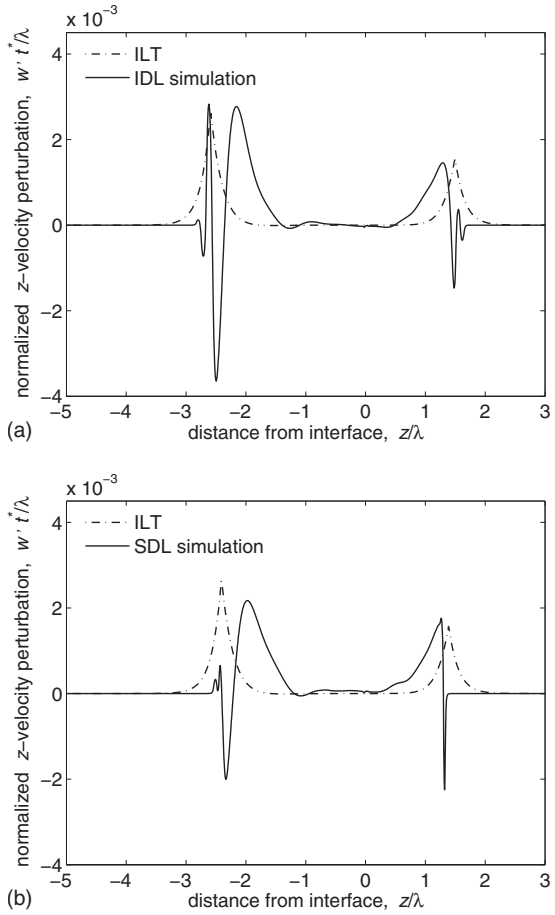

FIG. 14. Profiles of w at $x=0$ in the reference frame of the interface at $t/t^*=2$ from the ILT and (a) IDL and (b) SDL simulations corresponding to a shock accelerated interface with $M=1.1$, $\rho_2/\rho_1=3$, $\eta_0/\lambda=0.01$, $\gamma=5/3$, and $\beta=1$.

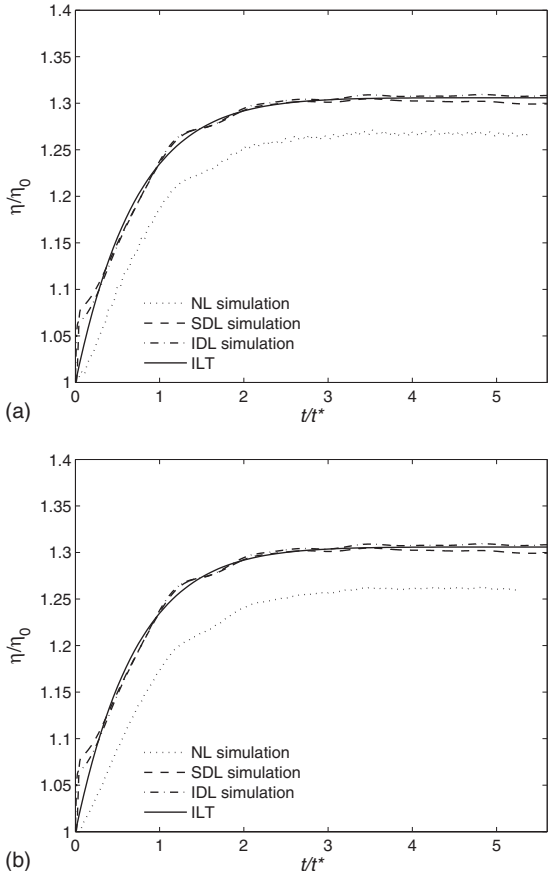

FIG. 15. Interface amplitude histories from the ILT, IDL, SDL, and NL compressible simulations corresponding a shock accelerated interface with $M=1.1$, $\beta=16$, $\rho_2/\rho_1=3$, $\gamma=5/3$, and (a) $\eta_0/\lambda=0.025$ or (b) $\eta_0/\lambda=0.1$.

This situation is different from all the cases examined so far and has serious consequences for the performance of ILT. Figure 14 shows profiles of w or w', as appropriate, in the reference frame of the interface from ILT and the linearized simulations of the $\beta=1$ case. The initial pressure in the IDL simulation is set to the postshock interaction pressure p_4, as stated in Sec. III C. At this pressure $\beta=1.341\,43>6/5$; thus a is still slightly greater than C_A. They are sufficiently close, however, that during the period when the interface is growing, information cannot propagate far enough upstream of the locations of the Alfvén fronts for a structure similar to that seen in ILT to form upstream of the front locations. This in turn significantly alters the downstream flow, as is evident in Fig. 14(a). In the shock driven simulations, the propagation speed of the outermost shocks is approximately the same as that of the Alfvén fronts in ILT. This results in constant interaction between the outermost shocks and the flow features that govern the overall evolution of the interface (which were reasonably well represented by ILT in the other cases) rather than the separation that was present in the cases examined previously. In both simulations, it can be seen from Fig. 14 that these factors cause the flow in the vicinity of the interface to deviate significantly from the ILT. Fitted values of η_∞ and σ from the $\beta=1$ simulations are shown in Table III, but in the shock driven cases the estimates are highly unreliable as η is still increasing at the end of the simulations. In summary, the performance of ILT is reasonable for weak magnetic fields but is compromised once the magnetic field becomes sufficiently strong that the Alfvén speed approaches the acoustic sound speed. Consequently, the ILT should not be used to estimate the behavior of the MHD RMI for cases where $C_A \geq a$.

D. Effect of increased perturbation amplitude

In this section the effect of increasing the initial perturbation amplitude η_0 is examined. This is done by studying two additional cases with $\eta_0/\lambda=0.025$ and $\eta_0/\lambda=0.1$. The other parameters are the same as in the baseline case. Additional linearized simulations are not required for these cases as η_0 is scaled out of the linear problem. η/η_0 histories for these cases are identical to the baseline case. Figure 15 shows the η histories from ILT and the three simulations for the $\eta_0/\lambda=0.025$ and $\eta_0/\lambda=0.1$ cases (refer to Fig. 6 for the $\eta_0/\lambda=0.01$ case). The values of η_∞ and σ computed from these are shown in Table IV. From Fig. 15, it can be seen that the primary effect of increasing η_0 is to increase the percentage by which the impulsive ILT overpredicts the growth rate of the interface in the NL simulation. This effect has also been documented by Cook *et al.*[14] for the hydrodynamic Rayleigh–Taylor instability. The increasing overprediction of

TABLE IV. Interface perturbation parameters from the ILT and simulations corresponding to a shock accelerated interface with varying η_0/λ and $M=1.1$, $\beta=16$, $\rho_2/\rho_1=3$, and $\gamma=5/3$. For the NL simulations, $L_z=20\lambda$, $z_{if}=11.76\lambda$, $N_x=64$, $N_z=2560$, and $T_{sim}/t^*=5.6$.

η_0/λ	Model	IDL simulation	SDL simulation	NL simulation
η_∞/λ				
0.01	0.011 723 7	0.011 746 5	0.011 641 3	0.011 464 4
0.025	0.029 321 4	0.029 378 4	0.029 115 4	0.028 465 3
0.1	0.119 314	0.119 546	0.118 476	0.115 273
σt^*				
0.01	−1.389 82	−1.289 69	−1.420 71	−1.314 02
0.025	−1.389 82	−1.289 69	−1.420 71	−1.312 94
0.1	−1.389 82	−1.289 69	−1.420 71	−1.203 38

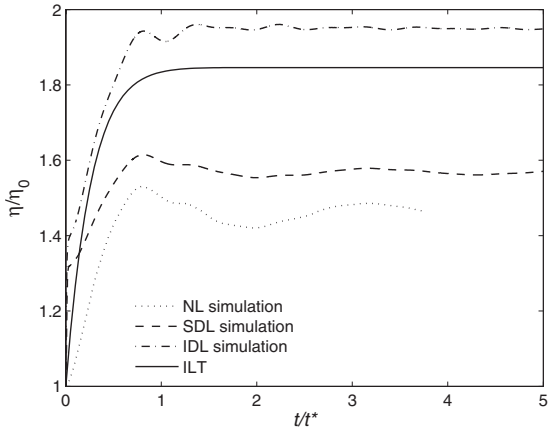

FIG. 16. Interface amplitude histories from the ILT and simulations corresponding to a shock accelerated interface with $M=2$, $\beta=1$, $\rho_2/\rho_1=3$, $\eta_0/\lambda=0.1$, and $\gamma=5/3$.

the growth rate by ILT results in the overprediction of the value of η_∞ observed in the NL simulation increasing from 2.2% to 2.9% to 3.4% as η_0/λ is increased from 0.01 to 0.025 to 0.1. The overprediction of σ, however, does not increase monotonically; it changes from 7.8% to 5.5% then 13.4% as η_0 is increased. Overall, the performance of the model slowly degrades as the initial perturbation amplitude is increased, as is expected for a linear model. Comparing the results presented in this section to those in Secs. IV B and IV C, it appears that the performance of ILT is less sensitive to increases in η_0 than it is to increases in either M or B; the error in η_∞ increases by only 1.2% as η_0 is increased by an order of magnitude.

E. Combined case

In this section, the performance of the ILT is assessed for the case where $M=2$, $\beta=1$, $\eta_0/\lambda=0.1$, $\rho_2/\rho_1=3$, and $\gamma=5/3$. This case represents what would appear to be the worst combination of the parameter values investigated in Secs. IV B–IV D from the perspective of model accuracy. The linearized simulations of this case were carried out in the domain $-20\lambda \le z \le 20\lambda$, which was discretized into $N_z=6400$ control volumes. The simulations were run for $N_t=8000$ time steps with a CFL number of 0.5. These simulations were run for a longer duration than for the other cases in order to examine the long period oscillations for more than 1 cycle. For the NL simulation of this case, $L_x=\lambda/2$, $L_z=12\lambda$, $z_{if}=3.4\lambda$, $N_x=128$, and $N_z=3072$. The simulation was run for the duration $T_{sim}/t^*=5$, which is approximately $5t_{99}$. Figure 16 shows the η histories from ILT and the three simulations for the current case. The values of η_∞ and σ computed from these are shown in Table V.

Comparing Figs. 16 and 13(b), it appears that there is better agreement between the ILT and the simulations of the present case than for the $M=1.1$, $\eta_0/\lambda=0.01$, and $\beta=1$ case. This is confirmed by the smaller fractional deviations in σ from the predicted value in the simulations of the present case. The improved agreement is due to the higher incident shock Mach number in the present case. In the IDL simulation, this increases the initial pressure so that a is significantly greater than C_A, allowing information to propagate further upstream of the Alfvén front locations. In the shock driven simulations, stronger outermost transmitted and reflected shocks are generated, which propagate significantly faster than the Alfvén fronts in the ILT, reducing the interaction that limited the accuracy of ILT in the $M=1.1$ case. This allows ILT to better predict the flow in the vicinity of the interface. The results for this case indicate that for strong shocks, large initial perturbations, and strong magnetic fields, the ILT may still give a rough estimate of the interface behavior, but it is not quantitatively accurate.

V. CONCLUSIONS

In order to assess the performance of the ILT of the MHD RMI developed by Wheatley *et al.*,[7] predictions from the ILT were compared to the results of IDL, SDL, and NL compressible MHD simulations for a variety of cases. The performance of ILT was first assessed for a baseline case with $M=1.1$, $\eta_0/\lambda=0.01$, $\beta=16$, $\rho_2/\rho_1=3$, and $\gamma=5/3$. For this case, the agreement between ILT and the interface behavior from the IDL simulation is excellent, with the model predicting the final amplitude of the interface to within 0.2%. Compressible waves present in the simulation caused small amplitude, short period oscillations in the amplitude of the interface that are not present in the ILT. These waves do not affect the overall evolution of the interface as they have no vorticity associated with them. The agreement between ILT and the SDL simulation is also excellent, while the final interface amplitude from the NL simulation is overpredicted by 2.2%. For all simulations of this case, ILT represents the flow structures that dominate the evolution of the interface with reasonable accuracy. In the shock driven simulations, the in-

TABLE V. Interface perturbation parameters from the ILT and simulations corresponding to a shock accelerated interface with $M=2$, $\beta=1$, $\rho_2/\rho_1=3$, $\eta_0/\lambda=0.1$, and $\gamma=5/3$.

	Model	IDL simulation	SDL simulation	NL simulation
η_∞/λ	0.109 167	0.115 32	0.092 858 7	0.086 842 8
σt^*	−3.754 05	−2.869 94	−4.180 7	−5.06429

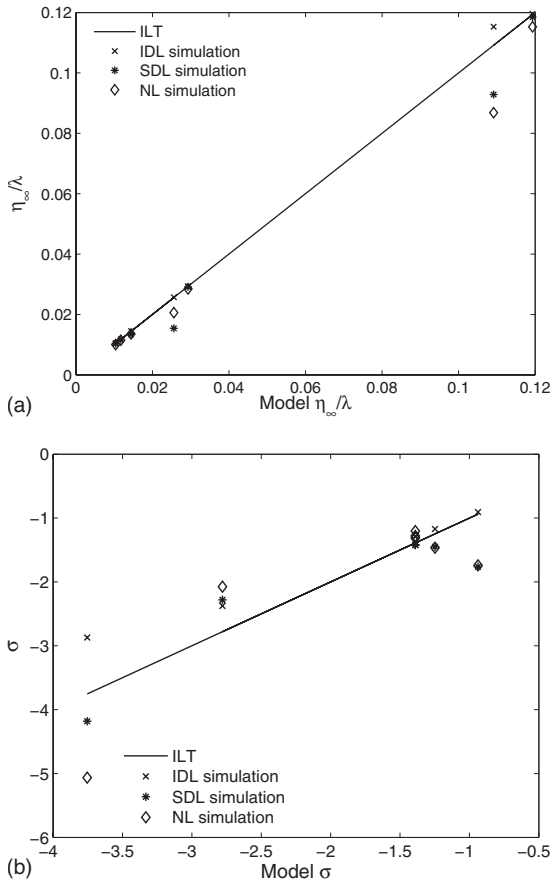

FIG. 17. Interface perturbation parameters η_∞ and σ from all NL, SDL, and IDL simulations vs the values predicted by the ILT.

terface amplitude also exhibits a long period oscillation caused by the interaction of transverse waves behind the shocks or outgoing waves reflected from the shocks. When the incident shock Mach number M is increased, the ILT still accurately predicts the behavior of the interface in the IDL simulation, but it increasingly overestimates the amplitude of the interface η in the shock driven cases. The amplitude of the long period oscillations in the shock driven simulations increases with M. As the nondimensional strength of the magnetic field β^{-1} is increased, ILT less accurately predicts the results of all simulations. The accuracy of ILT was found to be compromised once the magnetic field is sufficiently strong that the Alfvén wave speed approaches the acoustic sound speed, particularly if the incident shock is weak. When this occurs, the features of the flow that dominate the evolution of the interface deviate significantly from ILT. One such case with $\beta=1$ and $M=1.1$ was investigated. When initial perturbation amplitude of the interface η_0 is increased, the agreement between ILT and the linearized simulations is unchanged. The degree to which the ILT overpredicts η from NL simulations gradually increases with η_0.

The performance of ILT for all cases investigated, other than the case with $\beta=1$ and $M=1.1$ where reliable statistics could not be calculated, is summarized in Fig. 17. This shows the values of the final interface amplitude η_∞ and the time constant for the saturation of the interface σ that were calculated from the simulations plotted against the values predicted by ILT. It can be seen that the ILT collapses the data from the simulations well. In conclusion, the interface behavior given by the ILT well approximates that seen in compressible linearized simulations when $M-1$, η_0/λ, and β^{-1} are small. For such cases, the agreement with interface behavior that occurs in NL simulations is also reasonable. When $M-1$, η_0/λ, and β^{-1} are increased, the ILT becomes less accurate. For strong shocks, large initial perturbation amplitudes, and strong magnetic fields, ILT may give a useful estimate of the interface behavior, but it is not quantitatively accurate.

ACKNOWLEDGMENTS

V. Wheatley and D. I. Pullin were supported by the Academic Strategic Alliances Program of the Accelerated Strategic Computing Initiative (ASCI/ASAP) under Subcontract No. B341492 of DOE Contract No. W-7405-ENG-48. R. Samtaney was supported by U.S. DOE Contract No. DE-AC02-09CH11466.

[1] M. Brouillette, "The Richtmyer-Meshkov instability," Annu. Rev. Fluid Mech. **34**, 445 (2002).
[2] J. D. Lindl, R. L. McCrory, and E. M. Campbell, "Progress toward ignition and burn propagation in inertial confinement fusion," Phys. Today **45**(9), 32 (1992).
[3] D. Arnett, "The role of mixing in astrophysics," Astrophys. J., Suppl. Ser. **127**, 213 (2000).
[4] R. Samtaney, "Suppression of the Richtmyer-Meshkov instability in the presence of a magnetic field," Phys. Fluids **15**, L53 (2003).
[5] V. Wheatley, D. I. Pullin, and R. Samtaney, "Regular shock refraction at an oblique planar density interface in manetohyrodynamics," J. Fluid Mech. **522**, 179 (2005).
[6] J. T. Cao, Z. W. Wu, H. J. Ren, and D. Li, "Effects of shear flow and transverse magnetic field on Richtmyer-Meshkov instability," Phys. Plasmas **15**, 042102 (2008).
[7] V. Wheatley, D. I. Pullin, and R. Samtaney, "Stability of an impulsively accelerated density interface in magnetohydrodynamics," Phys. Rev. Lett. **95**, 125002 (2005).
[8] R. D. Richtmyer, "Taylor instability in shock acceleration of compressible fluids," Commun. Pure Appl. Math. **13**, 297 (1960).
[9] R. Samtaney, "A method to simulate linear stability of impulsively accelerated density interfaces in ideal-MHD and gas dynamics," J. Comput. Phys. **228**, 6773 2009.
[10] K. G. Powell, P. L. Roe, T. J. Linde, T. I. Gombosi, and D. L. DeZeeuw, "A solution-adaptive upwind scheme for ideal magnetohydrodynamics," J. Comput. Phys. **154**, 284 (1999).
[11] P. Colella, "Multidimensional upwind methods for hyperbolic conservation laws," J. Comput. Phys. **87**, 171 (1990).
[12] G. Toth, "The $\nabla\cdot B=0$ constraint in shock-capturing magnetohydrodynamics codes," J. Comput. Phys. **161**, 605 (2000).
[13] V. Wheatley, "On the Richtmyer-Meshkov Instability in Magnetohydrodynamics," Ph.D. thesis, California Institute of Technology, 2005.
[14] A. W. Cook, W. Cabot, and P. L. Miller, "The mixing transition in Rayleigh-Taylor instability," J. Fluid Mech. **511**, 333 (2004).